



City Research Online

City, University of London Institutional Repository

Citation: Pornsuwancharoen, N., Youplao, P., Aziz, M. S., Ali, J., Amiri, S., Punthawanunt, S., Yupapin, P. & Grattan, K. T. V. (2018). In-situ 3D Micro-sensor Model using Embedded Plasmonic Island for Biosensors. *Microsystem Technologies*, 24(9), pp. 3631-3635. doi: 10.1007/s00542-018-3798-1

This is the accepted version of the paper.

This version of the publication may differ from the final published version.

Permanent repository link: <https://openaccess.city.ac.uk/id/eprint/19152/>

Link to published version: <https://doi.org/10.1007/s00542-018-3798-1>

Copyright: City Research Online aims to make research outputs of City, University of London available to a wider audience. Copyright and Moral Rights remain with the author(s) and/or copyright holders. URLs from City Research Online may be freely distributed and linked to.

Reuse: Copies of full items can be used for personal research or study, educational, or not-for-profit purposes without prior permission or charge. Provided that the authors, title and full bibliographic details are credited, a hyperlink and/or URL is given for the original metadata page and the content is not changed in any way.

City Research Online:

<http://openaccess.city.ac.uk/>

publications@city.ac.uk

In-situ 3D Micro-sensor Model using Embedded Plasmonic Island for Biosensors

N. Pornsuwancharoen¹, P. Youplao¹, M.S. Aziz², J. Ali², I.S. Amiri³, S. Punthawanunt⁴, P. Yupapin^{5, 6*}, K.T.V. Grattan⁷

¹Department of Electronics Engineering, Faculty of Industry and Technology, Rajamangala University of Technology Isan, Sakon Nakhon Campus, Sakon Nakhon, 47160, Thailand;

²Physics Department, Faculty of Science, Universiti Teknologi Malaysia, 81310 Johor Bahru, Malaysia;

³Division of Materials Science and Engineering, Boston University, Boston, MA, 02215, USA;

⁴Interdisciplinary Research Center, Faculty of Science and Technology, Kasem Bundit University, Bangkok 10250, Thailand;

⁵Computational Optics Research Group, Advanced Institute of Materials Science, Ton Duc Thang University, District 7, Ho Chi Minh City, Vietnam;

⁶Faculty of Electrical & Electronics Engineering, Ton Duc Thang University, District 7, Ho Chi Minh City, Vietnam;

⁷Department of Electrical & Electronic Engineering, School of Mathematics, Computer Science & Engineering, City,

University of London, Ec1V 0HB, United Kingdom;

*Corresponding author E-mail: preecha.yupapin@tdt.edu.vn

Abstract:

The design of the microsensor system for biosensors using the plasmonic island is proposed. The sensor head is formed by the stacked layers of silicon-graphene-gold materials. The dual-mode operations of the sensor can be performed using the relationship of the changes between the electron mobility and optical phase, where the exciting environment can be light intensity(phase), electrical transient, heat, pressure, flavour and smoke, The change in light phase(intensity) in silicon and conductivity(mobility) in gold layers cause change in the output measurands. The design and simulation interpretation of the sensor is presented. The sensor manipulation using the MCM arrangement is simulated and interpreted for biosensor applications 3D imaging can also be applied to the MCM function, where the 3D in situ sensor function is possible. The sensor sensitivity of $2.0 \times 10^{-21} \text{ cm}^2 \text{ V}^{-1} \text{ s}^{-1} (\text{mW})^{-1}$ via simulation is obtained.

Keywords: Microring sensors; Biosensors; Enviromental sensors; Plasmonic sensors; 3D sensors; Dual-mode sensors

1. Introduction

Plasmonic materials and devices have been widely investigated and used in many aspects of theoretical and experimental works [Ozby, 2006; Aldawsari et al., 2015; Felidj et al., 2005; Eurenus et al., 2008; Xiao et al., 2006]. The major aspect of the current is the transformation relationship between the electromagnetic wave and electron energies that can be used to take the required measurement. Sensor-based on a plasmonic material is also an interesting device [Ali et al., 2018; Pornsuwancharoen et al., 2017], which can be used in either optical or electron electrical operation by using the relationship between the electron and light energies. There are many research articles published on the investigation of plasmonic sensors [Feng et al., 2011; Morrill et al., 2010; Li et al., 2016; Hasan et al., 2018; Anker et al., 2008], which have shown the advantages of various forms of devices and applications. The integrated plasmonic devices have shown the good potential for biosensing applications [Ren-Bing et al., 2013; Pornsuwancharoen et al., 2017], where one of them is formed by the plasmonic island within the modified add-drop filter, in which the induced changes in the electron mobility and light intensity(phase) can be relatively measured and the relationship established. This means that sensitivity of the device sensor can be worked out. In this work, the plasmonic island is integrated within the Panda-ring resonator to form a biosensor. The plasmonic island is formed by the stacked layers of silicon-graphene-gold materials, which is found to be very promising for light-electron energy conversion that can be applied to sensor application. Principally, light energy is initially input into the stacked device via a silicon core, which is a well-established technique [Gall, 2016; Baccarani and Ostojica, 1975]. The plasmonic waves are introduced into the graphene layer via the silicon layer input light, the excited electrons occur within the gold layer, which can be dived by the external output sorce by the required applications.. Moreover, the input and output of such layers can be the

optical or electrical signals, while the medium of both applications is the light fields that can be coupled by either electrons or photons. In this article, we have designed a system that can be used to detect the change in the electrical or optical quantities, especially, intensity(or phase) of light or electrical mobility(of current) for the specific points . We are presenting a simulation based investigation, however, the used parameters are closed to the existing device fabrication technologies. By using the graphical method using Optiwave, followed by the mathematical simulation via Matlab program, the problem can be easily solved and the simulation results obtained. The sensor manipulation is demonstrated by changing the reflection coefficients of the microring conjugate mirror material, which is the TiO2 [Wang et al., 2003; Faruki et al., 2016]. The change in the relationship between the electron mobility and the input power due to the stimuli environment of the sensor system is the sensor sensitivity. The 3D image of the activity between the sensor and the stimuli is formed by the add port output, which is the FWM output of the MCM, in which the 3D image can be formed by the 3D imaging recovery system [Phattharacorn et al., 2016; Phattharacorn et al., 2018; Chaiwong et al., 2017].

2. Background

We understand that mathematical complexity is not necessary to obtain simulation results. By using graphical approach, the required parameters can be acquired and used in the existing equations. Simple mathematical formulae can be used to obtain required results. In this work, the whispering gallery mode is the required of the system shown in Figure 1(a, b). The acquired parameters are then be used to perform the mathematical simulations. The optical field (E) propagates through the microring system as shown in Figure 1(a) is given by equations (1)-(3) [Phattharacorn et al., 2016; Amiri et al., 2012].

$$\mathbf{E}_z = \mathbf{E}_{i1} = \mathbf{E}_0 e^{-ik_z t - \omega t} \quad (1)$$

Where E_0 is the electric field amplitude (real), \mathbf{k}_z is the wave number in the direction of propagation and ω is the angular frequency.

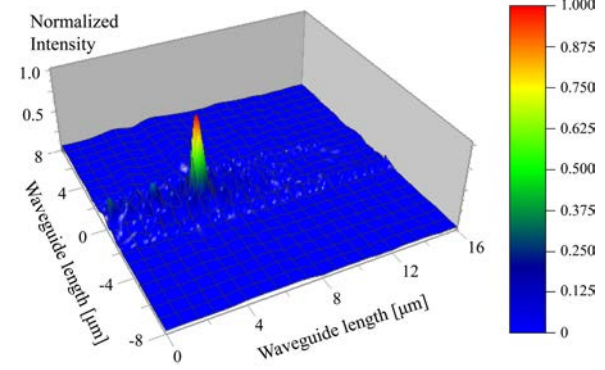
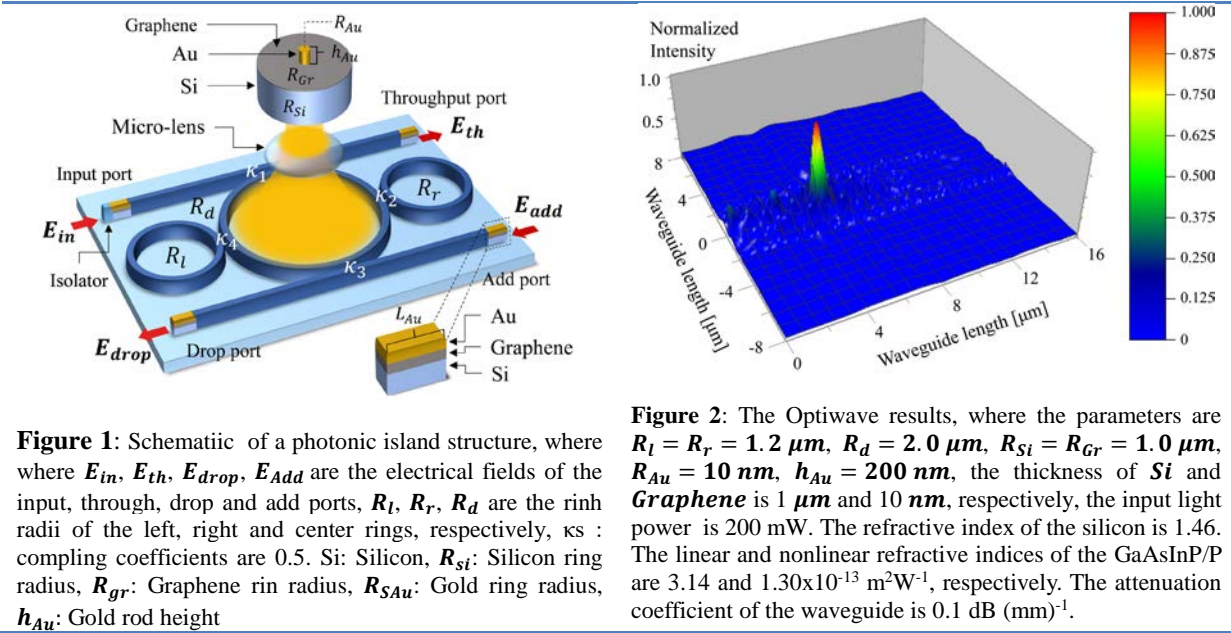
$$\mathbf{E}_{t1} = A\mathbf{E}_{i1} - B\mathbf{E}_{i2} e^{\frac{-\alpha L}{2} - jk_n \frac{L}{2}} \left[\frac{CE_{i1} \left(e^{\frac{-\alpha L}{2} - jk_n \frac{L}{2}} \right)^2 + DE_{i2} \left(e^{\frac{-\alpha L}{2} - jk_n \frac{L}{2}} \right)^3}{1 - F \left(e^{\frac{-\alpha L}{2} - jk_n \frac{L}{2}} \right)^2} \right] \quad (2)$$

$$\mathbf{E}_{t2} = x_2 y_2 \mathbf{E}_{i2} \times \left[\frac{x_1 y_2 \sqrt{\kappa_1 \kappa_2} E_{0r} E_{i1} \left(e^{\frac{-\alpha L}{2} - jk_n \frac{L}{2}} \right) + x_1 x_2^2 y_1 y_2 \sqrt{\kappa_2} E_{0r} E_{0L} E_{i2} \left(e^{\frac{-\alpha L}{2} - jk_n \frac{L}{2}} \right)^2}{1 - x_1 x_2 y_1 y_2 E_{0r} E_{0L} \left(e^{\frac{-\alpha L}{2} - jk_n \frac{L}{2}} \right)^2} \right] \quad (3)$$

Where $x_1 = \sqrt{1 - \gamma_1}$, $x_2 = \sqrt{1 - \gamma_2}$, $y_1 = \sqrt{1 - \kappa_1}$, $y_2 = \sqrt{1 - \kappa_2}$, $A = x_1 x_2$, $B = x_1 x_2 y_2 \sqrt{\kappa_1} E_{0L}$, $C = x_1^2 x_2 \kappa_1 \sqrt{\kappa_2} E_{0r} E_{0L}$, $D = (x_1 x_2)^2 y_1 y_2 \sqrt{\kappa_1 \kappa_2} E_{0r} E_{0L}^2$, $F = x_1 x_2 y_1 y_2 E_{0r} E_{0L}$. The other positions of the electrical field outputs within the system can also be found, where the mathematical formulas are to be found the give reference [Phattharacorn et al., 2018]. Under specific conditions, add port output can be observed due to reflection (feedback), where in this work the TiO2 lengths are used to obtain the required optical power reflection [Chaiwong et al. 2017; Phattharacorn et al., 2018]. However, the energy conservation of the system must be satisfied, hence, the normalized system is applied, where the normalized condition of the the input and output power for the remaining power. The remain output from the other ports are always found.

The 3D image construction, reconstruction and display is also presented in this work, which can be performed by using the same system which is considered as the microring conjugate mirror(MCM). Phattharacorn et al. [Phattharacorn, et al., 2016], report that the MCM can be formed when the reflected power from the through and drop ports are suitably selected. The image construction can be seen at the WGM output, while the image reconstruction is obtained at the add port. In case of remote image transmission, the link of the fiber optic cable is required, from which the output of the add port is input into the input port and displayed at the WGM output, which produces naked-eye perception. The proposed sensor can be used as the dual-mode sensor, which means that the applied external source can have optical or electrical parameters. The two modes are the optical or electrical modes that can be selected by different output detection systems, which are obtained by the quantity in terms of the optical phase term as $\varphi = \frac{2\pi \Delta n_{eff} L}{\lambda}$, where Δn_{eff} is the change in the effective refractive index, L is the optical path difference, and λ is the input source wavelength. The relationship between the light intensity (I), group velocity and the electron mobility can be expressed as $\mathbf{I} = \mathbf{E}^2 = \left(\frac{V_d}{\mu} \right)^2$, which is defined by $V_d = \mu E$. When an electric field E is applied to the grating sensor and an electric current is established in the conductor. The density J_s of this current is given by $J_s = \sigma E$. The constant of proportionality σ is called the

specific conductance or electrical conductivity of the conductor (gold is $1.6 \times 10^8 \text{ W}^{-1} \text{ m}^{-1}$) [Gall, 2016; Baccarani and Ostoja, 1975]. The advantage of the modified add-drop filter with two side rings is that the nonlinear effect can offer the shorter output pulse width and easier WGM resonant output control than the original system [Phatharacorn et al., 2017; Pornsuwancharoen et al., 2017]. The sensitivity of the system can be obtained by the relationship between the electron mobility output and the applied current (input power). Moreover, the use of the proposed sensor system may be possible for biosensors, specifically, using gold nanoparticles for the detection of viruses (cells) [He et al., 2011; Lee et al., 2015; Foreman et al., 2015; Sharma and Dominic, 2018; Anker et al., 2008].



3. Manipulation and Results

In a simulation, the manipulation of the proposed plasmonic circuit for biosensor with the 3D image presentation has been configured by using the change in the MCM reflected power. The used parameters satisfy the practical microring parameters and the waveguide supported Q-factor [Bogaerts et al., 2012]. The TiO₂ coated lengths on the waveguide ends at the throughput and drop ports were varied, which is configured as the change in the sensing mechanism during the measurement. The in-situ 3D image of the sensing mechanism can be captured and the image displayed by the naked-eye 3D imaging recovery. The used parameters are provided with the given in the related figure captions and the following content. The plot of the add port mobility visibility output with the reflected end TiO₂ lengths from 100-600 nm is shown in Figure 3. This is the MCM output is obtained from the sensor unit, which is the reflected information of the image construction at the sensor head, which is shown the relationship between the mobility visibility output and the different TiO₂ lengths. It will be selected to perform the required sensor sensitivity. The electron mobility in a gold material is $42.6 \text{ cm}^2 \text{ V}^{-1} \text{ s}^{-1}$ [Gall, 2016; Baccarani and Ostoja, 1975], the electron mass is 9.10×10^{-31} kilograms, the electron charge is 1.60×10^{-19} coulombs. The refractive index of the silicon is 1.46. The linear and nonlinear refractive indices of the GaAsInP/P are 3.14 and $1.30 \times 10^{-13} \text{ m}^2 \text{ W}^{-1}$, respectively. The attenuation coefficient of the waveguide is $0.1 \text{ dB} (\text{mm})^{-1}$. The plot of relationship between the mobility output and input power of the through, drop and add ports is shown in Figure 4 is obtained by using the Equations (1)-(3) with the MATLAB program, where the source wavelength is $1.55 \mu\text{m}$, the TiO₂ coated end length is 100 nm, the input power is varied from 0.5-5.0 mW. The other parameters are given in Figure 2. There are 6 points (pixels) of 3D images of the sensor activity manipulation by varying the TiO₂ end lengths shown in Figure 5. The add port outputs are used to form the 3D images by entering the optical output signal into the 3D image recovery system, which is the same system with the input information as shown in Figure 1. The selected plotted six TiO₂ length and WGM power variations are plotted, where (a) 600 nm, 0.1 mW, (b) 500 nm, 0.12 mW, (c) 400 nm, 0.2 mW, (d) 300 nm, 0.25 mW, (e) 200 nm, 0.3 mW, (f) 100 nm, 0.34 mW. The 3D images of the six different parameters and images are seen. The sensor head is the stacked layers of silicon-graphene-gold materials as shown in Figure 1, which means that if there is any change of light power or electron mobility related quantities introduced into the sensor system, will affect to the mobility output at all ports, while the 3D images of the measured target sample can be in-situ display. This system can be

integrated with the microscale device regime that can be used for cells or molecules sensors, while the live monitoring can be performed. In application, the MCM array can be integrated and the number of 3D pixels increased for large volume display.

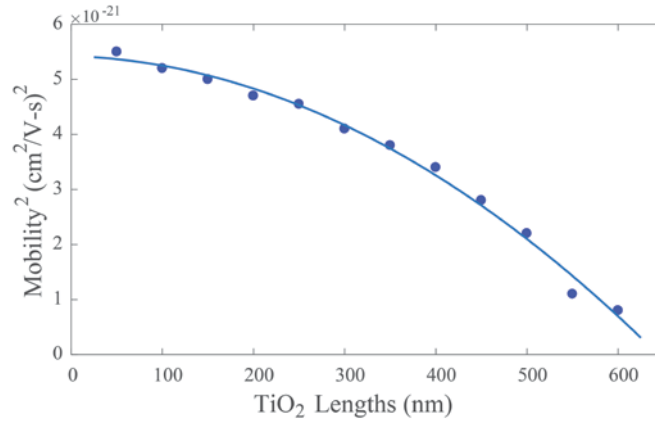


Figure 3: The plot of the add port mobility visibility output with the reflected end TiO₂ lengths, which was varied from 100-600 nm using the MATLAB program. The data points are the simulation result, where the solid line is the fitting curve.

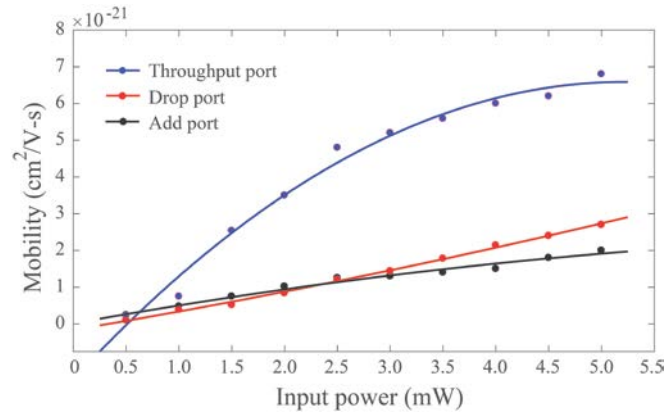


Figure 4: The plot of the mobility output and input power of the through, drop and add ports at the source wavelength of 1.55 μm , using the Equations (1)-(3) with the MATLAB program. The data points are the simulation results, where the solid lines are the fitting curves. The throughput and drop ports have shown the linear relationship, the sensor sensitivity $2.0 \times 10^{-21} \text{ cm}^2 \text{ V}^{-1} \text{ s}^{-1} (\text{mW})^{-1}$ is obtained.

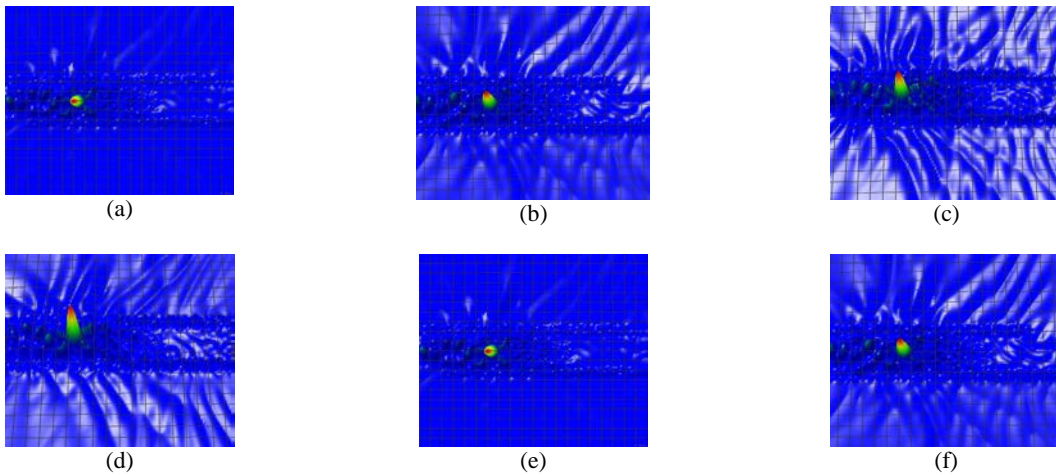


Figure 5: Plots of the sensor activity manipulation by varying the TiO₂ end lengths, using the Optiwave program. The add port outputs are plotted with the six TiO₂ length and WGM power variations, where (a) 600 nm, (b) 500 nm, (c) 400 nm, (d) 300 nm, (e) 200 nm, (f) 100 nm. The 3D images of the six different measurement values are plotted and seen, which is the manipulation of the sensing data.

4. Conclusion

We have proposed the use of the plasmonic island embedded within the MCM for the in situ 3D biosensors. The amount of change in cells quantities in response to the optical or electrical quantities tells about sensitivity of the sensor. We have manipulated the excited sensor environments by changing the MCM reflection coefficients to employ the sensor quantities. By the manipulating simulation, we have found that the change in the sensor head can be occurred by the exciting environment related to the electron mobility or light incident energy. For an instant, the change in cells quantities related to the optical or electrical quantities can be formed the sensor sensitivity. We have manipulated the excited sensor environments by changing the MCM reflection coefficients to employ the sensor performance. The in-situ 3D image is also possible formed and presented by the output of the MCM, where the FWM signal outputs are input into the display system, the 3D image of the sensor is confirmed and displayed. The sensor sensitivity of $2.0 \times 10^{-21} \text{ cm}^2 \text{ V}^{-1} \text{ s}^{-1} (\text{mW})^{-1}$ is obtained. Moreover, this system is not required the electronic 3D image reconstruction, it is the naked-eye 3D display using the image recovery, which is the same as the initial input system.

Acknowledgment:

M.S. Aziz would like to acknowledge the support and facilities through Flagship UTM Shine Project (03G82). P. Yupapin would like to acknowledge for the research facilities to Ton Duc Thang University, Vietnam. This is Prof. Ali UTM Shine cost center number is Q.J130000.2426.03G82 (Flagship UTM Shine).

References

- Aldawsari, S., Wei, L., Liu, W.K., 2015. Theoretical study of hybrid guided modes in a multilayer symmetrical planar plasmonic waveguide, *J. Lightw. Technol.*, 33(15), 3198-3206.
- Ali, J., N. Pomsuwancharoen, Youplao, P., Aziz, M.S., Chiangga, S., Jaglan, J., Amiri, I.S., and P. Yupapin, 2018. A novel plasmonic interferometry and the potential applications, *Results in Physics*, 8, 438-411.
- Amiri, I.S., Ali, J. and Yupapin, P.P., 2012. Enhancement of FSR and finesse using add/drop filter and panda ring resonator, *J. Mod. Phys. B* 26, 1250034.
- Anker, J.N., Hall, W.P., Lyandres, O., Shah, N.C., Zhao, J. and R.P. Van Duyne, R.P., 2008. Biosensing with plasmonic nanosensors, *Nat Mat.*, 7(6), 422-453.
- Baccarani, G. and Ostojic, P. 1975, Electron mobility empirically related to the phosphorus concentration in silicon, *Solid State Electron.*, 18(6), 579-580.
- Bogaerts, W., Heyn, P.D., Vaerenbergh, T.V., Vos, K.D., Selvaraja, S.K., Claes, T., Dumon, P., Bienstman, P., Chaiwong, K., Tamee, K., Punthawanunt, S., Suhailin, F. H., Aziz, M. S., Ali, J., Singh, G. and Yupapin, P., 2017. Naked-eye 3D imaging model using the embedded micro-conjugate mirrors within the medical micro-needle device. *Microsystem Technologies* 12(1), 1-5.
- Hourhout, D.V. and Baets, R. 2012. Silicon micro-ring resonators, *Laser Photon. Rev.*, 6(1), 47-73.
- Eurenius, L., Haggglund, C., Olsson, E., Kasemo, B. and Chakarov, D., 2008. Grating formation by metal-nanoparticle-mediated coupling of light into waveguided modes, *Nature Photonics*, 2, 360-364.
- Faruki, M.J., Razak, M.Z.A., Azzuhri, S.R., Rahman, M.T., Soltanian, M.R.K., Rahman, B.M.A., Grattan, K.T.V., Rue, R.D.L. and Ahmad, H., 2016. Effect of titanium dioxide (TiO₂) nanoparticle coating on the detection performance of microfiber knot resonator sensors for relative humidity measurement, *Material Express*, 6, 501-508.
- Felidj, N., Laurent, G., Aubard, J., Levi, G., Hohenau, F.A., Krenn, J.R. and Aussenegg, F.R., 2005. Grating-induced plasmon mode in gold nanoparticle, *J Chem. Phys.*, 123(22), 221103.
- Feng, J. V., Siu, S., Roelke, A., Mehta, V., Rhieu, S.Y., Tayhas, G., Palmore, R., Pacifici, D., 2011. Nanoscale plasmonic interferometers for multispectral, high-throughput biochemical sensing, *Nano Lett.*, 12(2), 602-609.
- Foreman, M.R., Swaim, J.D. and Vollmer, F., 2015. Whispering gallery mode sensors, *Adv. Opt. and Photon.*, 7, 168-240.
- Gall, D., 2016, Electron mean free path in elemental metals, *J Appl. Phys.*, 119, 085101.
- Hasan, Md. R., Akter, S., Rifat, A.A., Ahmed, K., Ahmed, R., Subbaraman, H., Abbott, D., 2018. Spiral photonics crystal fiber-based dual-polarized surface plasmon resonance biosensor, *IEEE Sensors Journal*, 18(1), 133-140.
- He, L., Ozdemir, S.K., Zhu, J., Kim, W. and Yang, L., 2011. Detection single viruses and nanoparticles using whispering gallery microlasers, *Nature Nanotechnology*, 6, 428-432.
- Lee, M.Y., Jackson, A.O. and Lee, L.K., 2015. Bioinspired optical antennas: gold plant viruses, *Light; Science & Applications*, 4, e267.
- Li, D., Feng, J., Pacifici, D., 2016, Nanoscale optical interferometry with incoherent light, *Scien. Rep.*, 2016, Article number 20836.
- Morrill, D., Li, D. and Pacifici, D., 2010, Measuring subwavelength spatial coherence with plasmonic interferometry, *Nature Photonics*, 10, 661-687.
- Ozbay, E., 2006. Plasmonics: merging photonics and electronics at the nanoscale dimensions, *Science*, 311(5738), 189-193.

- Phattharacorn, P., Chiangga, S., Ali, J. And Yupapin, P., 2018, Micro-optical probe model using integrated triple microring resonators for vertical depth identification, *Microsystem and Technologies*, Accepted.
- Phattharacorn, P., Chiangga, S. and Yupapin, P., 2016. Analytical and simulation results of a triple micro whispering gallery mode probe system for a 3D blood flow rate sensor, *Appl. Opt.*, 55(33), 009504.
- Phatharaworamet, T., Teeka, C., Jomtarak, R., Mitatha, S. and Yupapin, P.P., 2010. Random binary code generation using dark-bright soliton conversion control within a Panda Ring resonator, *J Lighthwave Technol.*, 28(19), 2804-2809.
- Pomsuwanchaoren, N., Youplao, P., Amiri, I.S., and P. Yupapin, P., 2017(a). Electron driven mobility model by light on the stacked metal-dielectric-interfaces, *Microw. & Opti. Techn. Lett.*, 59(7), 1704-1709.
- Pomsuwanchaoren, N., Amiri, I.S., Suhailin, F.H., Aziz, M.S., Ali, J., Singh, G. and Yupapin, P., 2017(b). Micro-current source generated by a WGM of light within a stacked silicon-graphene-Au waveguide, *IEEE Photon. Technol. Lett.*, 29(21), 1768-1771.
- Ren-Bing, T., Hua, Q., Xiao-Yu, Z., Wen, X., 2013, Electronics driven plasmon dispersion in AlGaIn/GaN high electron mobility transistors, *Chin. Phys. B*, 22(11), 117306.
- Sharma, A.K. and Dominic, A., 2018. Influence of chemical potential on graphene-based SPR sensor's performance, *IEEE Photonics Technology Letters*, 30(1), 95-98.
- Xiao, J.J., Yakubo, K. and Yu, K.W., 2006. Optical switching in graded plasmonic waveguides, *Appl. Phys. Lett.*, 88, 241111.
- Wang, W. and Y. Ku, Y., 2003. The light transmission and distribution in an optical fiber coated with TiO₂ particles, *Chemosphere*, 50(8), 999-1006.